

University of Arkansas, Fayetteville

ScholarWorks@UARK

---

Mechanical Engineering Undergraduate Honors  
Theses

Mechanical Engineering

---

12-2018

## Photochemical Etching of Nitrided Stainless Steel Piston Rings

Steven Sonntag

*University of Arkansas, Fayetteville*

Follow this and additional works at: <https://scholarworks.uark.edu/meeguht>



Part of the [Manufacturing Commons](#), [Service Learning Commons](#), and the [Tribology Commons](#)

---

### Citation

Sonntag, S. (2018). Photochemical Etching of Nitrided Stainless Steel Piston Rings. *Mechanical Engineering Undergraduate Honors Theses* Retrieved from <https://scholarworks.uark.edu/meeguht/77>

This Thesis is brought to you for free and open access by the Mechanical Engineering at ScholarWorks@UARK. It has been accepted for inclusion in Mechanical Engineering Undergraduate Honors Theses by an authorized administrator of ScholarWorks@UARK. For more information, please contact [scholar@uark.edu](mailto:scholar@uark.edu), [uarepos@uark.edu](mailto:uarepos@uark.edu).

# Photochemical Etching of Nitrided Stainless Steel Piston Rings

# Photochemical Etching of Nitrided Stainless Steel Piston Rings

A thesis submitted in partial fulfillment of  
the requirement for the Mechanical Engineering  
Honors Program

By

Steven Sonntag

November 2018  
Department of Mechanical Engineering  
College of Engineering  
University of Arkansas  
Fayetteville, AR

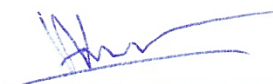
Thesis Director:



---

Dr. Min Zou

Thesis Committee:



---

Dr. Arun Nair

## Acknowledgements

I would like to thank Dr. Min Zou for her advice, support, and patience as the advisor for this project, as well as Dr. Arun Nair for serving on the thesis committee.

Thank you to Josue “Josh” Goss for your guidance, technical support, and advice in the laboratory. Your help was invaluable to this project. This thanks is also extended to Shelby Maddox.

Funding for this project was provided by the Ford Motor Company and the National Science Foundation.

## Abstract

Piston rings are designed to provide a seal between the piston and the cylinder wall of internal combustion engines, keeping oil from the crankcase from getting into the combustion chamber. This means piston rings are the main point of contact between the piston and the cylinder wall, which causes the piston to experience high amounts of friction and wear. By texturing the surfaces of the cylinder wall and/or the piston ring, the amount of contact area can be reduced, allowing for less friction, slower wear, and better gas mileage. In this thesis experiments, photochemical etching processes were developed to etch nitrided stainless steel piston rings with designed geometrical patterns for the purpose of friction reduction. Studies were performed to investigate several types of photoresists, optimize the printing parameters for the photoresist AZ-9260, and to determine the etching rates of hydrochloric acid. The results showed that it is possible to accurately etch distinct shapes at the micro scale while controlling the etching depth. This research demonstrates the feasibility of texturing the flat side of piston rings through photochemical etching for the purpose friction reduction, and the research results provide a solid basis for future studies to further refine and apply the same techniques to selectively etch the curved surface of the piston ring.

**Key Words:** Photochemical Etching, Nitrided Stainless Steel Piston Rings, AZ-9260, Etch Rate

Contents	
Abstract	iv
1 INTRODUCTION AND BACKGROUND	1
1.1 Friction Reduction and Surface Texturing Techniques	1
1.2 Photolithography	3
1.3 Acid Etching and Acid Selection	4
2 EXPERIMENTAL DETAILS	5
2.1 Preliminary Experiments	5
2.1.1 Photoresist Selection and Optimization	5
2.1.2 Piston Ring Preparation Process	7
2.1.3 Optimization of Nanoscribe Printing Parameters and Printed Designs	9
2.3 Acid Etching Procedure	12
3 DATA AND RESULTS	13
4 CONCLUSIONS	25
5 FUTURE WORK	26
5.1 Dimple Shape, Size, and Depth	26
5.2 Material and Application	26
5.3 Friction Tests	26
References	27
APPENDIX	29

# **1 INTRODUCTION AND BACKGROUND**

## **1.1 Friction Reduction and Surface Texturing Techniques**

In the automotive sector, friction is a large problem. It is said that about 30% of the fuel consumed in internal combustion engines is used to overcome frictional forces within the engine itself [1-3]. Since the early 1900s, engineers have tried to reduce friction within the engine by modifying the surfaces of interacting parts. One such example is the practice of honing the engine cylinder [4]. There are multiple ways to hone an engine cylinder, but all honing methods have the same goal: to create 45-degree, cross-hatched groove patterns that will allow the engine oil to spread evenly on the entire surface of the cylinder wall [5]. With the oil creating a film between the piston ring and cylinder, wear and friction are reduced because of hydrodynamic lubrication [6,7].

Although honing is still widely practiced today, as technology advances, many other surface texturing techniques have been researched and experimented with, and most techniques successfully reduced friction. The most current research related to subtractive surface engineering is focused on creating surface textures through means of laser ablation [8-10], mechanical micro machining [11], deformation-based techniques, such as micro indentations [12], and photochemical machining, with the most sought after technique being laser ablation.

Laser ablation uses a focused, high-energy beam to vaporize specific shapes and patterns into a chosen surface. The advantage of this technique is that it is very accurate and takes relatively short amounts of time because of modern technological advances with the femtosecond laser. Laser ablation can be applied to most surface materials. Some disadvantages are that this technique requires very expensive equipment, and unless the laser is optimized correctly, or if



the laser is not strong enough, the material being targeted by the laser can be melted and redeposited on the surface of the material, creating burs and non-smooth surfaces [8]. It is also possible that the mechanical, chemical, and/or electrical properties of the area surrounding the texture being created by the laser can be changed due to the possible high heat created by the laser [13].

Traditional micromachining uses micro-drilling and micro-milling to remove material from the surface of a material [14,15]. These manufacturing techniques have some disadvantages, especially related to orbital revolving drills, such as radial run-out in the direction of centripetal motion and drill wear [11].

The micro indentation techniques are used to emboss specific patterns and shapes by application of pressure and the deformation of the surface. A tool is created with specific textures that is stamped on the surface and transfers the texture to the substrate. Some advantages of this process are the inexpensive tools required and the simplicity of this technique. Possible disadvantages could include the embossed material being mechanically pushed up to the surface of the substrate, much like the laser ablation, creating an uneven surface and burs, and material properties changing related to the mechanical deformation.

The technique being focused on for this thesis is photochemical machining. This process uses photolithography and acid etching to create textures in the surface of the substrate. Although this process requires potentially dangerous chemicals, it does not share the disadvantages of the aforementioned techniques, and it can be applied to any material.

## 1.2 Photolithography

Photolithography is essential in the fabrication process of integrated circuits [16]. To create circuits, a layer of photoresist must be deposited, cured, and developed, before etching takes place.

Photoresists can be categorized into two categories: positive or negative photoresists. Negative photoresist typically starts in liquid form, and once it is exposed to UV-light, it is cured or polymerized, becoming solid. Once the desired area of photoresist is cured, what is uncured can be removed to expose the underlying substrate. Positive photoresists typically have a liquid initial state. After it is applied to the substrate, it must be cured and solidified with heat. After it is cured, it can be exposed to UV light, depolymerizing the molecular structure resist. The UV-exposed region becomes more soluble in developer solutions and can be removed. The selection of the photoresist should be based on the UV exposure process, the desired shapes, and ratio of substrate area to be etched versus non-etched. After being developed, the region of exposed substrate should be the same size and shape of the photoresist that was exposed to UV light and removed.

After UV-exposing the photoresist and developing it, the material can be etched with either wet or dry techniques, which respectively employ liquid acid solutions or plasma. After being etched, depending on the application, a new layer of photoresist can be applied, or the resist can be completely removed to expose the entire substrate.

For this thesis experiments, a positive resist was used to minimize the time required for exposing the photoresist. This is because the etched areas cover less than 50% of the surface area of the piston ring substrate and a Nanoscribe photonic 3D printer, which selectively and

precisely exposes the photoresist with a focused laser, was used for a maskless lithography method.

### **1.3 Acid Etching and Acid Selection**

The selection of the acid used for the etching process should be based on the substrate being etched. For most etching related to photolithography, the targeted substrates are silicon wafer chips. The etchant commonly used for silicon is a hydrofluoric acid solution [17]. HF can also be used to etch stainless steel and other material, but due to the dangers associated with it and the laboratory that this research was performed in being unprepared to handle HF, a different etchant had to be found.

There are numerous publications that contain lists of different etching solutions and the substrate that the etchants can react with, such as the Handbook of Metal Etchants [18,]. In many lists, there are multiple solutions created to target either martensitic, austenitic, or ferritic stainless steels, or to target specific grain boundaries of the various stainless steels [19,20]. Most of these solutions are mixtures of alcohols, acids, water, and other materials, but due to the dangers associated with mixing acids and bases, most of these solutions were avoided. The most common component of these different solutions, regardless of targeted material, is hydrochloric acid [21]. For this reason, HCl was selected to etch the nitrided piston rings made of 17% Cr martensitic stainless steel.

## **2 EXPERIMENTAL DETAILS**

Sections 2.1 – 2.2 discuss the steps taken to perform the experiment. A full list of the equipment used for these experiments can be found in the appendix.

### **2.1 Preliminary Experiments**

#### **2.1.1 Photoresist Selection and Optimization**

For this thesis experiment, because of the shapes that were selected to be etched into the piston ring covering less than 50% of the surface area, and because a maskless lithography method was chosen, it was decided to use a positive photoresist to minimize the time required for exposing the photoresist. For the selection of the specific resist, application techniques on the flat side of the piston ring section were tested based on the transferability of the technique, for future research, to the curved surface of the piston ring.

Two different positive photoresists were initially tested: ADEX TDFS and AZ-9260. ADEX TDFS photoresist comes in flexible, solid sheets that are hot-rolled onto the substrate. These photoresist sheets were deemed unsuitable for the experiments due to difficulty with the application process; the success rate of applying the sheet to the curved surface of the piston ring had a 0% success rate of application and retention with lasting adhesion. AZ-9260 is initially a very viscous liquid, which is typically spin-coated onto the substrate and soft-baked before being exposed to UV-rays. Multiple tests were performed to discover the optimum technique to apply a coating of AZ-9260 with uniform thickness onto a piston ring section. Initial tests of spin coating the piston ring failed when attempting to uniformly coat the curved surface of the piston ring, and thus this technique was avoided. Multiple tests of spray-coating the piston ring with different diluted solutions of AZ-9260 also failed to provide a uniform protective layer. The

technique of dip-coating was chosen because both flat and curved surfaces can be dip coated with a uniform coating thickness.

Tests were performed to discover which dilution ratio and thickness of coating that was able to keep a piston ring section from being etched when submerged in HCl for 20 minutes. To prepare the solutions, AZ-9260 was mixed with PGMEA in ratios of 1:0 (pure AZ-9260), 3:1, 2:1, and 1:1. The thinnest coating was the 1:1 ratio of AZ-9260 to PGMEA, with an average coating thickness of 1.8 micron thick. Each larger concentration of AZ-9260 increases the thickness of the coating, to 4.9 microns, 6.9 microns, and up to 52.3 microns with pure AZ-9260.

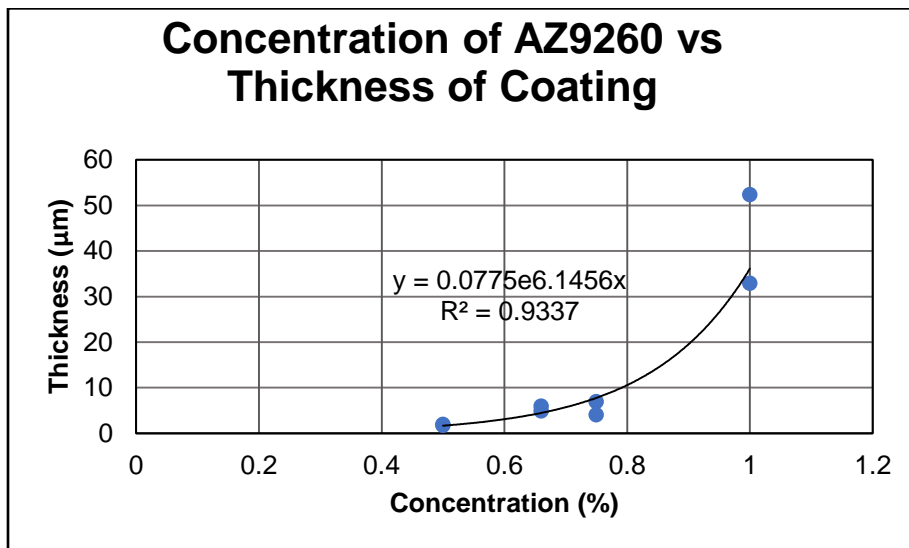


Figure 1: Graph with trend line showing AZ-9260 thickness based on concentration.

The thinnest solution was proven to be resistant to HCl for over 20 minutes, so it was assumed all thicker coatings would sufficiently protect the piston ring as well. A solution of 2:1 of AZ-9260 to PGMEA was selected.

### 2.1.2 Piston Ring Preparation Process

To prepare the piston rings for the experiments, many steps had to be initially taken. The piston rings were first cut into small sections, averaging 0.7cm in length, using a Dremel 8050-N/18 Micro 8V rotary tool with diamond tipped wheels. To do this, the piston ring must be clamped to a heat sink (a copper bar was used in these experiments). If no heat sink is used, the heat generated between the piston ring and the rotary tool will rise high enough to temper and discolor the piston ring.

The piston ring sections were then cleaned with the following steps: first, sonicate piston rings in a bath of hexanes, as per instructions from Ford, for 60 minutes. Then sonicate the ring sections in an acetone bath for 10 minutes, followed by an isopropyl alcohol bath for 10 minutes. Follow the IPA bath sonication with placing the rings in a plasma chamber for 1 minute at full power and 200 bar pressure.

Once the piston ring sections were properly cleaned, the PR sections were silanized with hexamethyldisilazane (HMDS). This is a necessary step to ensure adhesion of AZ-9260 on the piston ring during and after development, post UV exposure. To do this, a hose apparatus similar to Figure 2 will be required.

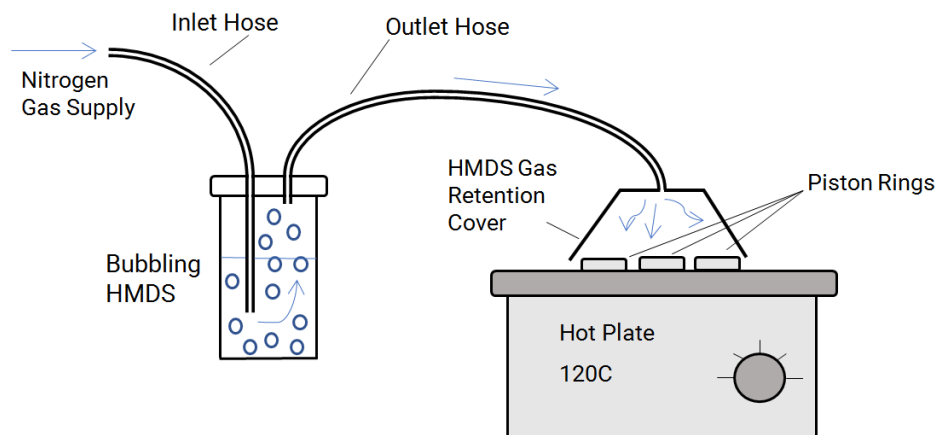


Figure 2: Setup for HMDS silanization of piston rings.

To set up the silanization process, a small container of HMDS was procured with two hoses going through the lid. The gas intake hose was pushed in to where the end reached the bottom of the container, allowing the nitrogen gas to bubble up through the HMDS, and the outlet hose was placed so the end inside the container was near the top, not too far below the lid. The other end of the outlet hose had a cup-like end piece, which fit over the piston ring sections, creating a small chamber for the piston rings to be encompassed by the HMDS gas.

Once setting up the apparatus, the inlet hose was connected to the nitrogen gas supply, and the piston rings were placed on a hot plate set to 120 °C. Once the piston rings reached 120°C, the rings were covered with the cup and the nitrogen gas supply was turned on. The gas supplied was opened enough so that the HMDS bubbled heavily. HMDS was deposited on the piston rings for 1 minute, and then the piston rings were flipped and the silanization process was repeated for another minute.

Once silanization was completed, the piston ring was dip coated in the 2:1 AZ-9260-PGMEA solution in a small beaker. For these experiments, only one side needed to be coated. In order to dip coat multiple piston rings at the same time, an array of ring sections were adhered to a piece of tape, making sure that the length from end to end of the piston ring rows did not surpass the depth of the beaker. The piston rings were lowered into the AZ-9260 solution at a rate of 10mm/minute. The rings were submerged for 3 minutes, and then raised out of the solution at a rate of 10mm/minute.

After dip coating the rings, they were placed on a hotplate set to 120 °C. The piston rings were baked for 10 minutes, and then allowed to cool and rehydrate in the air for at least 30 minutes. After allowing the AZ-9260 to rehydrate, they were prepared for the Nanoscribe. To do this, the rings were removed from the tape, and all residual resist on the side of the ring that

was attached to the tape was mechanically removed. A microscope glass was placed in the loading tray of the Nanoscribe, and a piece of double-sided tape was placed on the glass. The piston rings were then attached to the tape, with the coated face exposed to the air, and the loading tray inserted into the Nanoscribe for printing/UV exposure.

### **2.1.3 Optimization of Nanoscribe Printing Parameters and Printed Designs**

In order to decrease the complexity of the UV exposure process, it was decided to use a 20x magnification lens, so that an extra step of oil or glycerol emersion could be avoided; the 20x lens does not need fluid emersion, but the 25x lens and any higher magnification does.

The goal was set to make the printing as quick as possible while still maintaining the correct amount of UV exposure and the correct dimensions of the printed shapes. In the software, there were pre-set, optimized printing parameters for the 25x and the 63x lens, but not for the 20x lens. To perform the optimization, 4 different parameters had to be modified; core laser speed, core laser power, slicing distance (the vertical distance between each pass of the laser as it prints in the Z direction), and hatching distance (distance of the laser passes in the XY plane of printing). In this research, the slicing and hatching distances were changed in congruence, not individually.

The first tests performed were to discover which laser power and speed the 20x lens required. The printing parameters used were for those of the 25x lens, and 6x6 arrays of 50x50  $\mu\text{m}$  squares. The core laser power increased from 65% to 90% from left to right, and the core laser speed increased from 35,000 on the bottom row to 55,000 on the top row. The resulting shapes are seen in Figure 3.



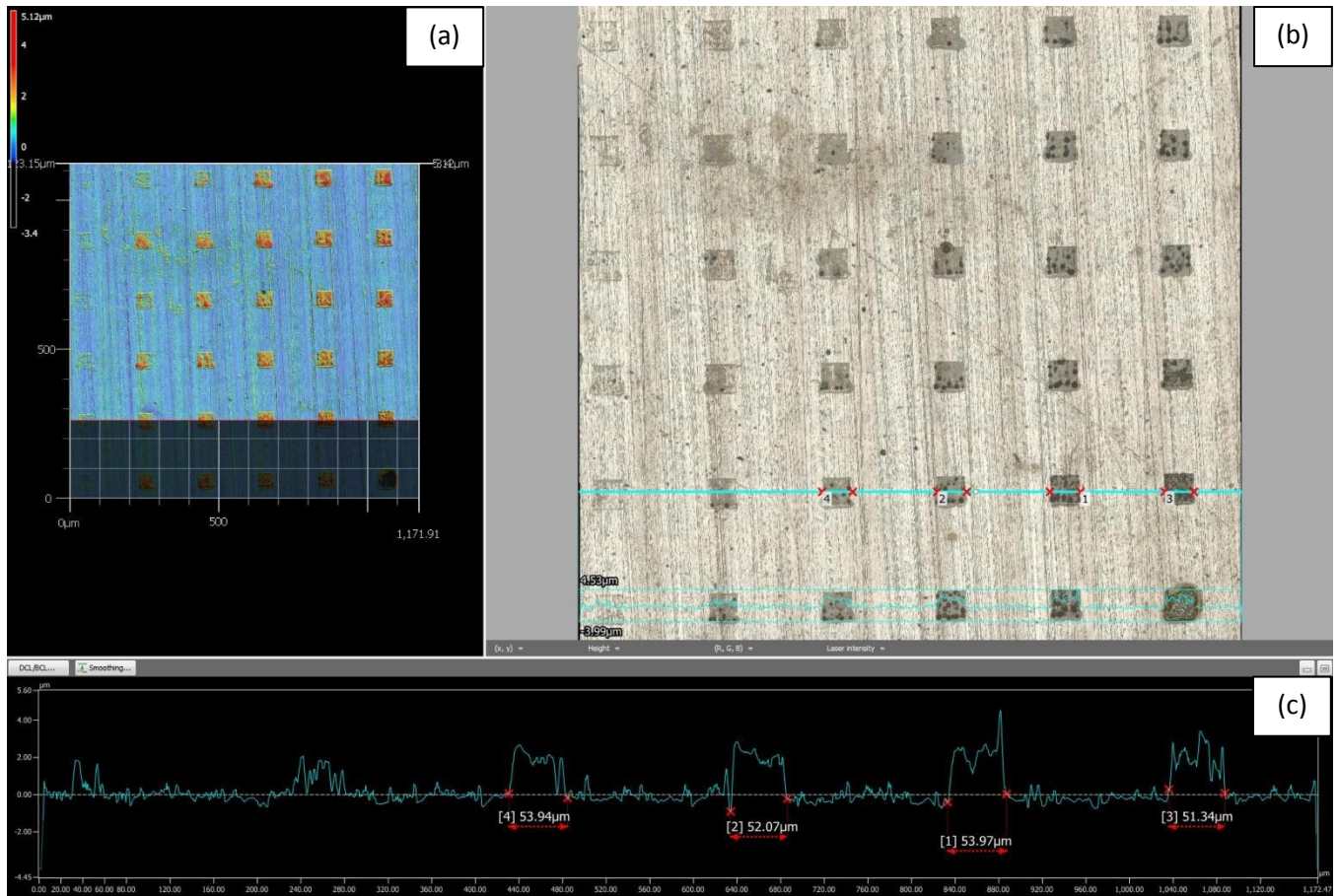


Figure 3: Keyence scan of the exposed photoresist from preliminary tests with the Nanoscribe to measure the accuracy of the exposure area compared to the designed shape. (a) is a height map of the scanned area, (b) is the optical image of the same area, (c) is the profile graph along the line seen in (b).

As seen in Figure 3, the Nanoscribe accurately exposed the photoresist. The average error associated with comparing the exposed area to the original design dimensions of the square was 6 to 7%.

Further tests were conducted to test hatching and slicing distances. The hatching and slicing distances used for the 25x lens were observed as 1  $\mu\text{m}$  and 0.5  $\mu\text{m}$ . The other two sets of printing parameters tested were a 1.25  $\mu\text{m}$  slicing distance with a 0.75  $\mu\text{m}$  hatching distance and a 1.5  $\mu\text{m}$  slice and a 1.0  $\mu\text{m}$  hatching distance. Along with testing the slicing and hatching parameters, laser speed and power were tested, in case the slicing and hatching had an effect on

required printing speed and laser power. For each set of slice and hatch parameters, 4x5 arrays of 50x50x30  $\mu\text{m}$  squares were created. From left to right in the array, power was increased in increments of 10 from 60% to 90% of full laser power, and from bottom to top, the core laser speeds were 35000, 40000, 45000, 50000, and 55000. The different arrays with each set of slicing and hatching distances were printed and developed for 5 minutes. Because the Keyence laser scanning microscope causes AZ-9260 to depolymerize, to see which printing parameter worked the best, the piston rings were developed and etched for 3 minutes in HCl and then scanned with the Keyence microscope scanner. The results are shown in Figure 4.



Figure 4: Optimization tests for printing parameters. Bottom left are two arrays for 1  $\mu\text{m}$  slicing and 0.5  $\mu\text{m}$  hatching distance. Middle two arrays represent the 1.25  $\mu\text{m}$  slicing distance with a 0.75  $\mu\text{m}$  hatching distance. Top right two arrays are for the 1.5  $\mu\text{m}$  slice and a 1.0  $\mu\text{m}$  hatching distance.

The squares were judged on the uniformity of the etching surface and the size and shape of the etched shape. Based on the above results, the printing parameters of 1  $\mu\text{m}$  slicing and 0.5  $\mu\text{m}$  hatching distance were selected, along with 50,000 core laser speed and 85% core laser power.

With the selected parameters, the shapes in Figure 5 were created to be printed for the etching experiment. Multiple shapes were put into the same arrays to minimize variations between printing jobs that may have been unknowingly introduced.

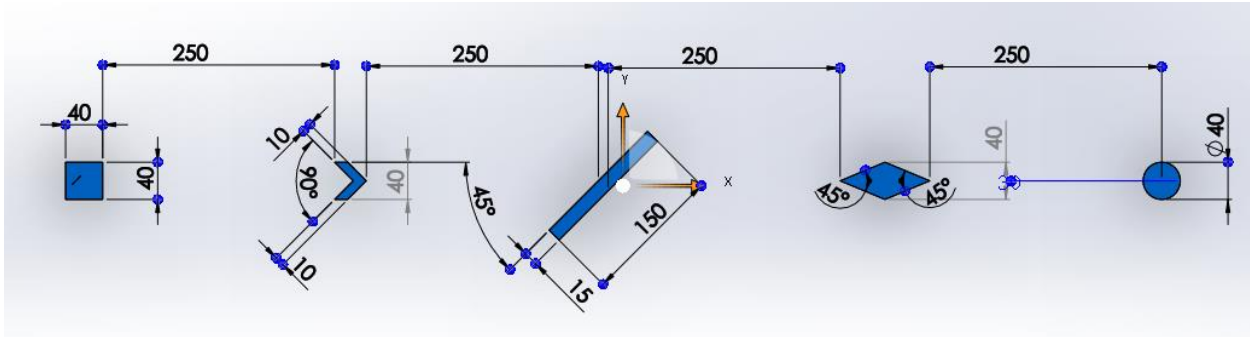


Figure 5: The various shapes and dimensions printed and tested with the Nanoscribe for acid etch testing. The square, chevron, diamond, and circle had a characteristic length of 40  $\mu\text{m}$ .

After the 3x5 arrays of the above shapes were printed, all piston rings were developed for 7 minutes in the 400K solution and were ready to be etched in acid.

### 2.3 Acid Etching Procedure

To observe the etching rate of HCl and how the shapes change over time, the following time steps were chosen for etching times: 3 minutes, 5 minutes, 8 minutes, 13 minutes, 19 minutes, 25 minutes, and 32 minutes. For each time step, one beaker of 40 mL was filled with 20 mL of HCl and a 25mL beaker was filled with DI water. For each time step, 3 piston ring sections were etched simultaneously in the beaker of acid. When the time for the etching ended, the acid was promptly poured into a waste container, and the rings simultaneously dropped into the beaker of water. The piston rings were rinsed 3 times with water, sonicated for 1 minute in water, rinsed 2 more times with water, sonicated for 5 minutes in acetone and 5 minutes in IPA, dried, then plasma treated for one minute before being scanned and imaged by the Keyence.

### 3 DATA AND RESULTS

After completing all etching trials, the piston rings were all scanned using a Keyence 3D LSM with a 20x lens, and the data was all collected with Keyence MultiFileAnalyzer software. All optical images and height maps can be found in the appendices of this paper.

The different etching time trials showed some very interesting data that is discussed below. The first observation that can be made is that the depths of all the shapes increase rather uniformly with each longer increment of etching time. Upon basic observation, it can also be seen that all shapes' depths are similar to one another, showing that the amount of area exposed to HCl does not change the rate of etching. This can be observed in the height map of a piston ring etched for 13 minutes, as well as the 2D profile across multiple shapes, seen in Figure 6.

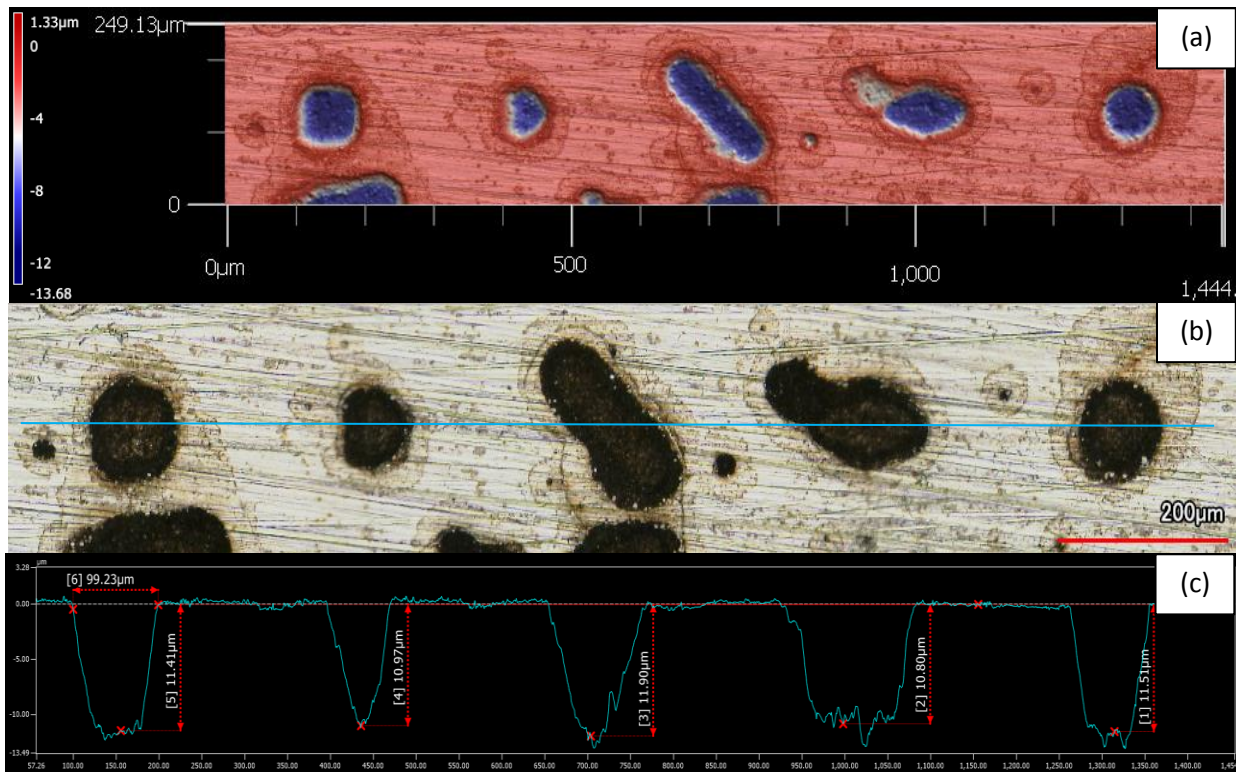


Figure 6: (a) 3D surface map of etched piston ring; (b) optical+laser image of same piston ring; (c) height profile graph of marked region of optical+laser image.

After collecting data on the average etch depth of all shapes for all time steps, the data collected was put into a table in excel for further analysis. It should be noted that the data for the 3-minute and 32-minute etching trials was ignored.

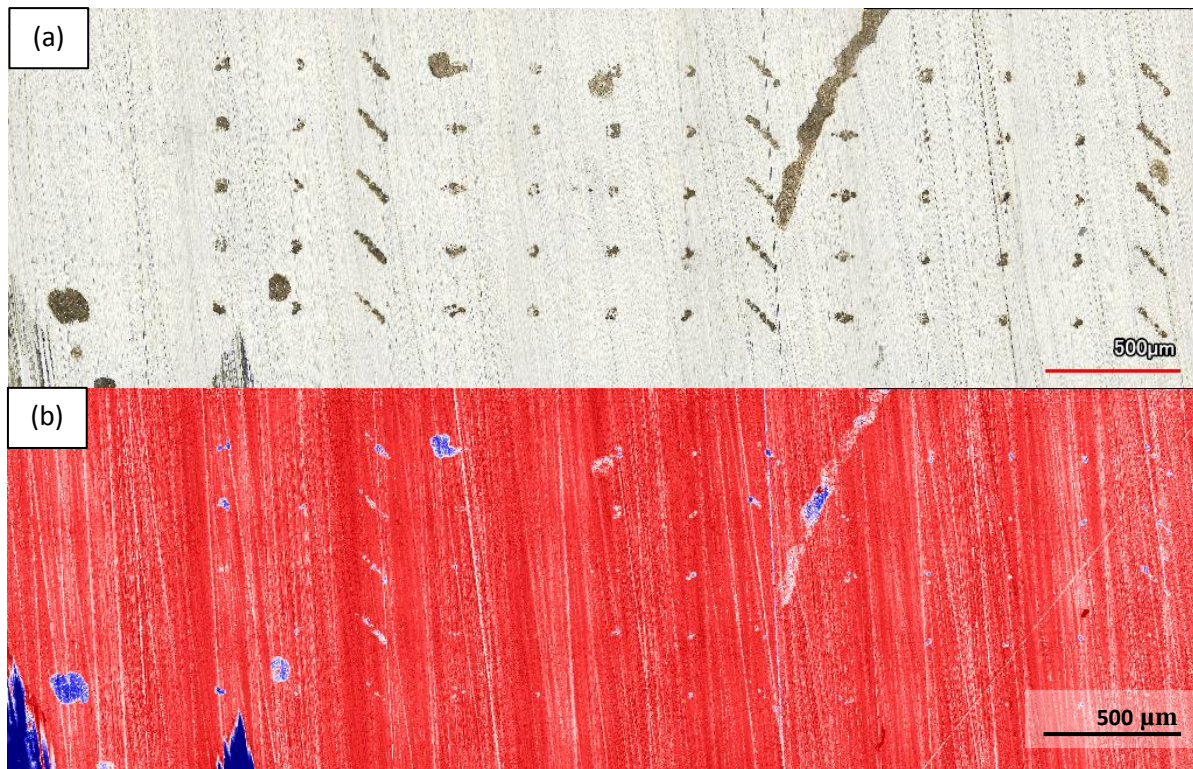


Figure 7: 3-Minute etching comparison of the optical results (a) and the height map (b).

For the 3-minute etching trials, although the etching is optically visible, most of the etching is difficult to analyze because pre-existing surface features are as deep and sometimes deeper than the etch depth of the shapes.

For the 32-minute trials, the etch depth easily observed, but due to the horizontal etching propagation, the shapes' boundaries exceeded the original spacing of 250  $\mu\text{m}$  between the individual shapes and all shapes began to interconnect. This can be observed in Figure 8.

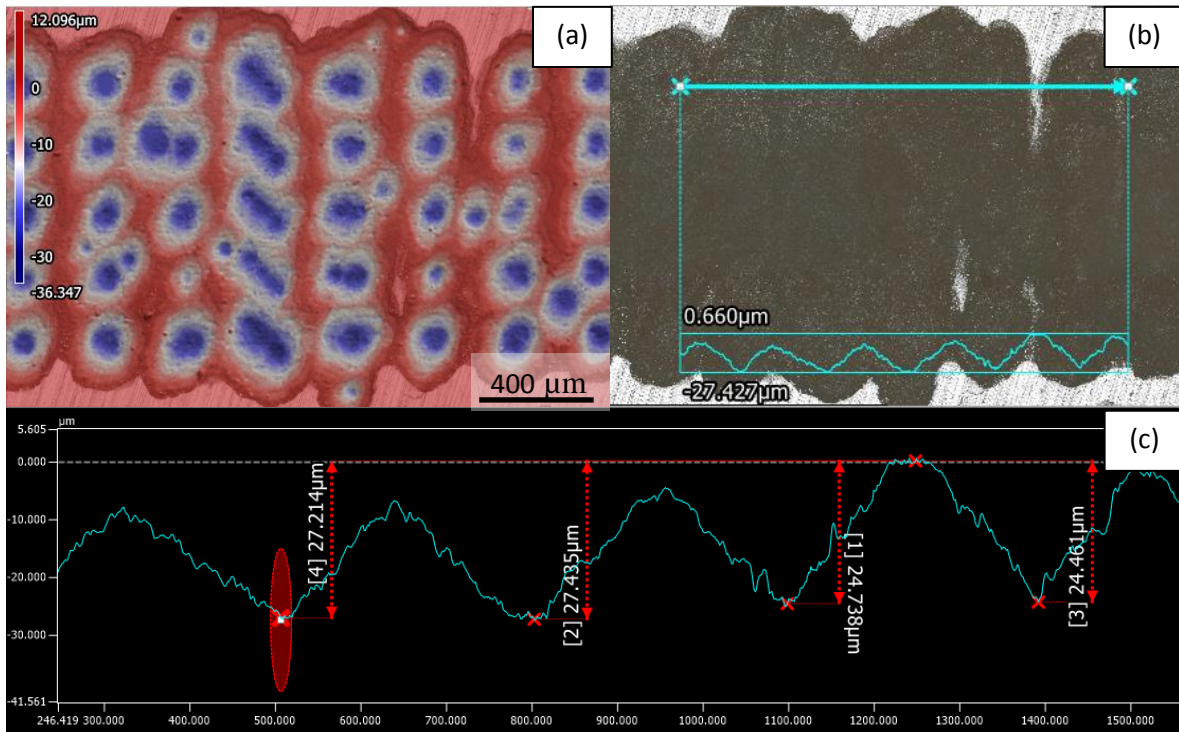


Figure 8: (a) 3D surface map; (b) optical+laser image; (c) height profile graph of 32-minute etching of same region of piston ring.

Table 1 shows the data of the etch depths across all shapes and time trials. The averages were found by using the Average Step Height tool in the MultiFileAnalyzer software. The un-etched surface was first selected to be the baseline, area 1, for each piston section. This is done by using the laser image, using the Ext Level selection tool, setting the tolerance to 5000, and the lightest colored pixel in a zoomed-in field of view. For area 2, the etched dimples, using the same process for area one, change the image to a height map, use the Ext level selection tool, set tolerance to 1.5  $\mu\text{m}$ , and select the deepest area etched on the piston ring. In Table 1, Average height is the average difference between area 1 and area 2 of the piston ring.

Time (minutes)	5	8	13	19	25
Average Etch Depth ( $\mu\text{m}$ )	-2.84	-5.38	-9.24	-12.55	-19.39
Std dev. Average Depth	0.64	0.45	2.86	0.43	5.24
Min Etch Depth ( $\mu\text{m}$ )	-2.20	-4.68	-8.53	-11.47	-18.42
Std dev. Min Depth	0.78	0.65	2.77	0.29	5.23
Max Etch Depth ( $\mu\text{m}$ )	-5.69	-8.01	-13.87	-16.12	-23.15
Std dev. Max Depth	0.21	0.35	2.78	1.75	5.73

Table 1: Average etch depths with standard deviation.

Figures 9 and 10 are all the data points plotted onto graphs. Figure 9 displays the average depth from the Table 1, and Figure 10 displays the minimum and maximum etch depths across all shapes on the piston rings, within the  $1.5 \mu\text{m}$  tolerance region. Trendlines were fitted to each data set along with the standard deviation. The equations matching each trendline set are displayed on the graphs.

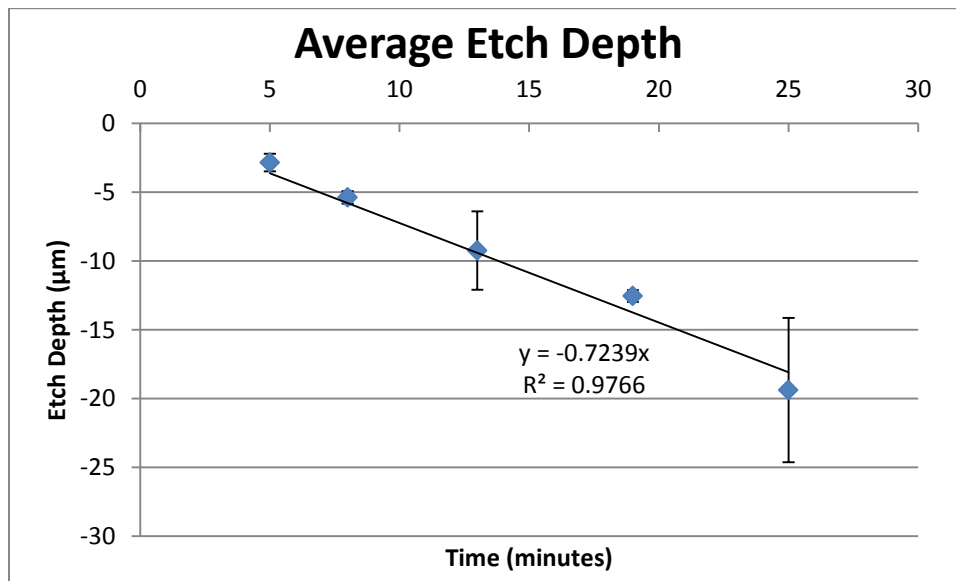


Figure 9: Average etch depth with Standard Deviation for each time step across all shapes.

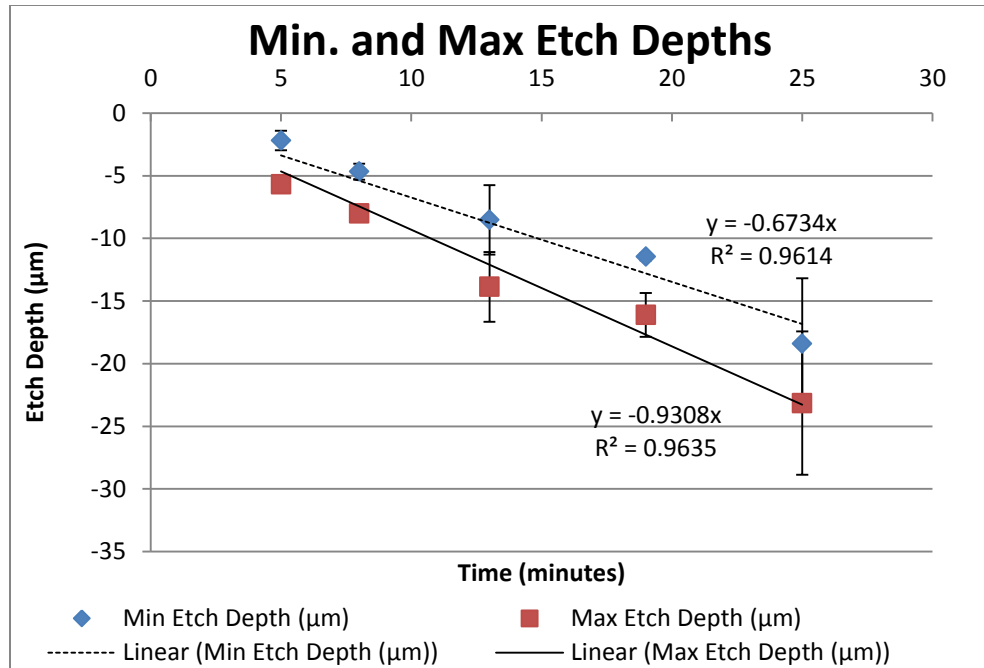


Figure 10: Minimum and maximum etch depths for all shapes in each time trial with standard deviation.

Along with vertical etch depth, horizontal etch propagation was measured for the square, rectangle, and diamond and tabulated in Tables 2-5. All shapes were measured, and the data points were culminated in Excel and plotted in Figure 11. The average length of the square sides are as follows: 57.17 μm for 5 minutes, 63.83 μm for 8 minutes, 94.45 μm for 13 minutes, 100.69 μm for 19 minutes, and 143.86 μm for 25 minutes. Based on the average lengths per time step and the designed length of 40 microns, the equation  $y = 3.8056x + 40$  can be extrapolated to calculate etched side length based on etch time, with y being the length of the square's side, and x being the etch time.



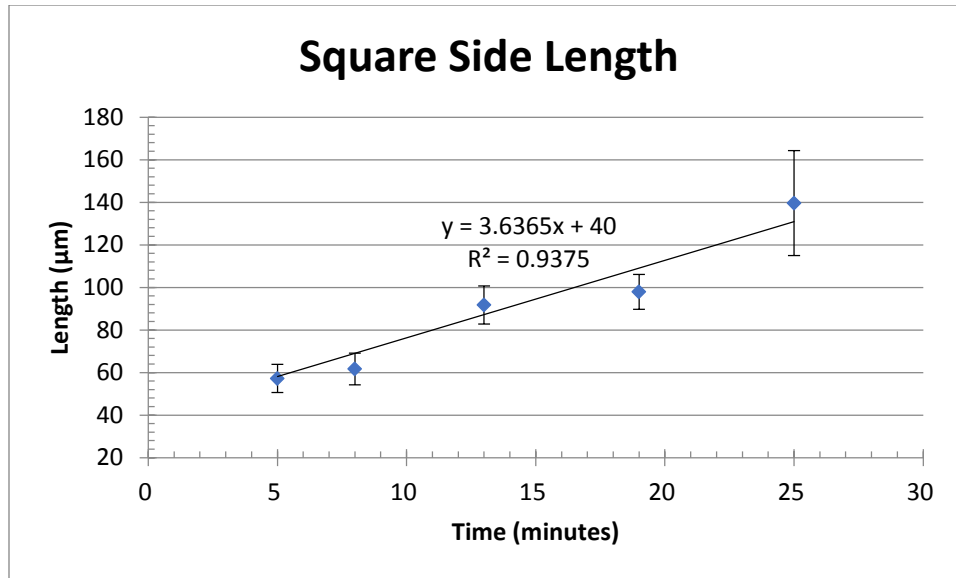


Figure 11: Change of square side length over time with standard deviation.

Statistical data related to all square side length measurements are displayed in Table 2. In the table, Q1 and Q3 represent the 1<sup>st</sup> and 3<sup>rd</sup> quartile of all measurements taken.

Square side length (µm)					
	5 minutes	8 minutes	13 minutes	19 minutes	25 minutes
Min	42.18	47.37	69.78	81.61	97.91
Q1	53.16	58.61	89.31	95.01	125.42
Med	57.55	64.56	94.84	100.50	140.31
Q3	61.32	67.48	101.41	107.09	167.20
Max	70.24	78.22	112.64	119.17	181.16
Average	57.17	63.83	94.453	100.69	143.86
Std. Deviation	6.61	7.47	8.94	8.19	24.67

Table 2: Statistical data for square side length measurements for each time step.

The rectangle that was tested had a large ratio of length to width, and it was discovered that the average length of the rectangle increased by almost 150%, from 169  $\mu\text{m}$  at 5 minutes, to 249  $\mu\text{m}$ , at 25 minutes. This is a small growth in comparison to the rectangles' width, which increased over 350%, from 38.5  $\mu\text{m}$  at 5 minutes, to 135  $\mu\text{m}$ , at 25 minutes. This leads to the belief that, although the amount of exposed surface area does not dramatically change the rate of etch depth, the amount of exposed area indeed changes the rate of horizontal etching propagation. The plots for rectangle length and width growth over time are seen Figures 12 and 13.

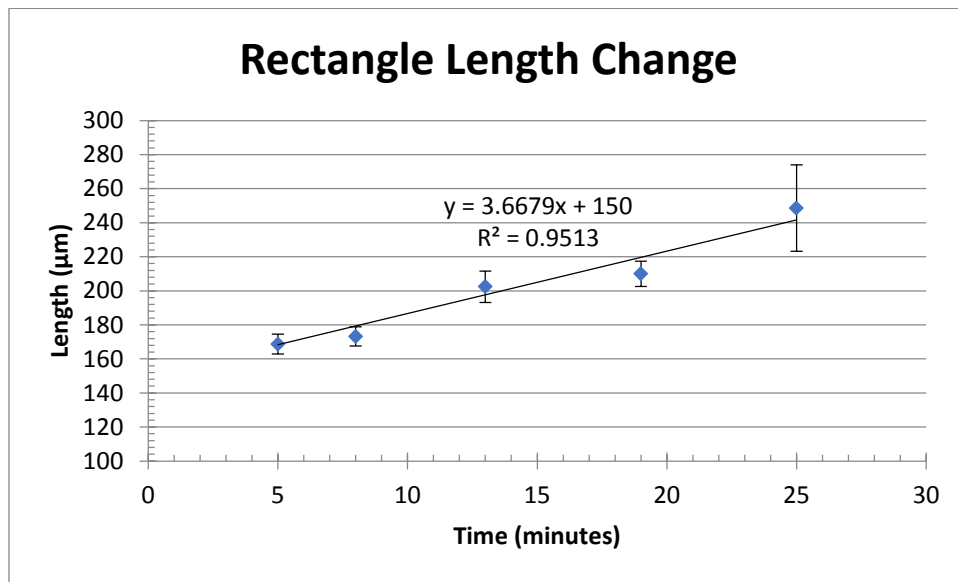


Figure 12: Rectangle length change over time. The average lengths of the rectangles for the time intervals of 5, 8, 13, 19, and 25 minutes are 168.71 $\mu\text{m}$ , 173.16 $\mu\text{m}$ , 202.39 $\mu\text{m}$ , 209.95 $\mu\text{m}$ , and 248.56 $\mu\text{m}$ , respectively.

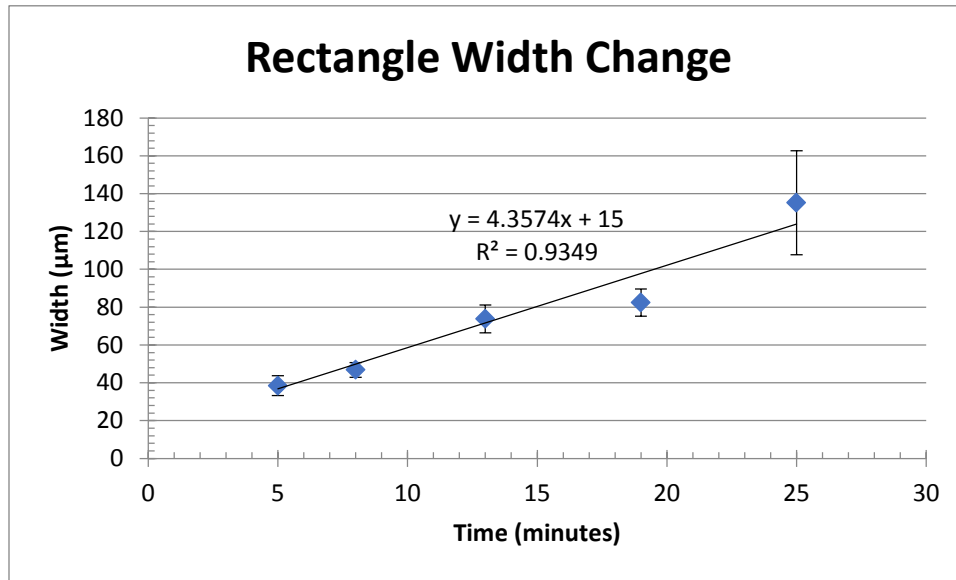


Figure 13: Rectangle Width change over time. The average widths of the rectangles for time intervals of 5, 8, 13, 19, and 25 minutes are 38.47µm, 46.8µm, 73.77µm, 82.43µm, and 135.14µm respectively.

The characteristic equation for calculating the rectangle’s length, based on an initial length of 150µm is  $y = 3.6679x + 150$ . For the width of the rectangle, with an initial width of 15 µm, the characteristic equation is  $y = 4.3574x + 15$ . These equations demonstrate the rate of growth of each dimension in the XY plane, meaning the width grows in a linear relation with time at a rate of more than 4 microns per minute, while the length increases at a rate of 3.67 microns per minute.

Table 3 displays statistical information related to all measurements taken of all rectangles’ widths and lengths.

(a) Rectangle Width (μm)					
	5 minutes	8 minutes	13 minutes	19 minutes	25 minutes
Min	29.31	40.29	61.05	60.34	90.13
Q1	33.56	44.02	69.21	79.83	107.06
Med	39.63	46.49	72.22	83.38	140.23
Q3	42.31	50.52	80.51	86.93	154.37
Max	48.18	52.56	84.39	95.33	183.24
Average	38.47	46.80	73.77	82.44	135.14
Std. Deviation	5.26	3.85	7.34	7.24	27.52

(b) Rectangle Length(μm)					
	5 minutes	8 minutes	13 minutes	19 minutes	25 minutes
Min	151.23	163.78	188.50	197.50	210.67
Q1	165.72	168.94	195.41	204.47	229.96
Med	169.22	174.38	201.20	209.27	246.22
Q3	173.48	176.66	211.11	216.64	262.17
Max	177.60	187.72	217.56	224.35	312.26
Average	168.71	173.16	202.39	209.95	248.56
Std. Deviation	5.86	5.65	9.18	7.46	25.39

Table 3: Statistical data for the rectangle etch width (a) and rectangle length measurements (b).

Along with the squares and rectangle characteristic lengths, the distances between the two obtuse angles of diamond shapes were measured and plotted in Figure 14. The distance between the obtuse angles of the diamond increased over time, starting at 55.67 μm for the 5-minute etch time and increasing to 60.74 μm, 89.47 μm, 96.35 μm, and 149.45 μm for the 8, 13, 19, and 25-minute etch times respectively. The characteristic equation for calculating the diamond's height, based on an initial distance between obtuse angles being 40μm is  $y = 3.7736x + 40$ , with x being time and y being characteristic length.

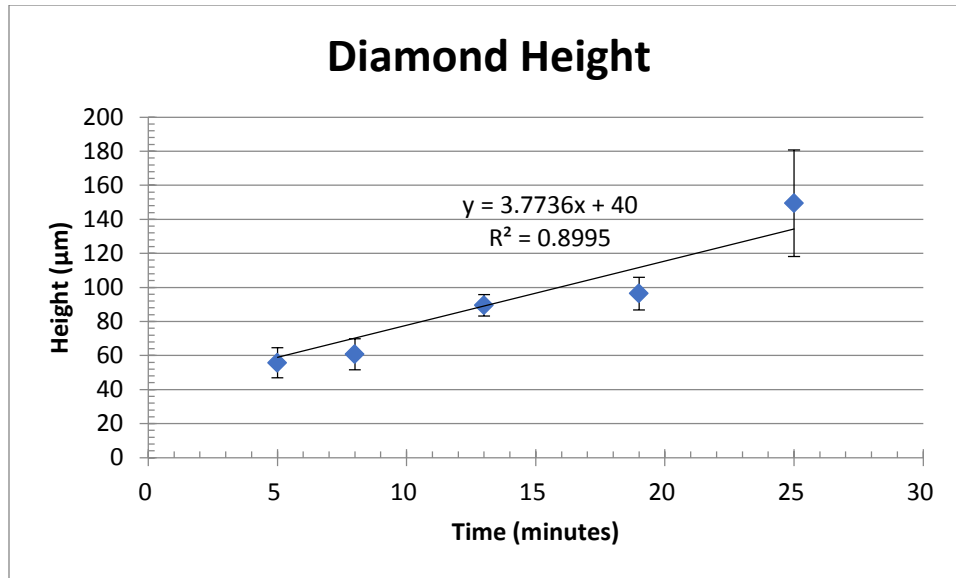


Figure 14: Change of Distance between obtuse angles over time.

Table 5 displays the same statistical information related to all diamond-height measurements at all time steps of etching.

Diamond Height(µm)					
	5 minutes	8 minutes	13 minutes	19 minutes	25 minutes
Min	37.44	43.16	75.87	79.37	95.98
Q1	51.70	56.65	85.01	88.29	125.02
Med	55.66	61.45	89.60	97.67	147.95
Q3	61.94	66.78	96.29	103.35	174.46
Max	72.32	76.24	98.72	115.94	208.75
Average	55.67	60.74	89.47	96.35	149.45
Std. Deviation	8.83	9.12	6.32	9.65	31.35

Table 4: Statistical Data on diamond height measurements.

Finally, it is worth noting that as the vertical and horizontal etch depth increased, the original characteristic shapes were still observable from 3 minutes to 13 minutes, but between 19 and 25 minutes, squares lost any semblance of a corner, diamonds became ovals, and chevrons

became rounded triangles. This can be observed in Figure 15 in the sample images of each time step below.

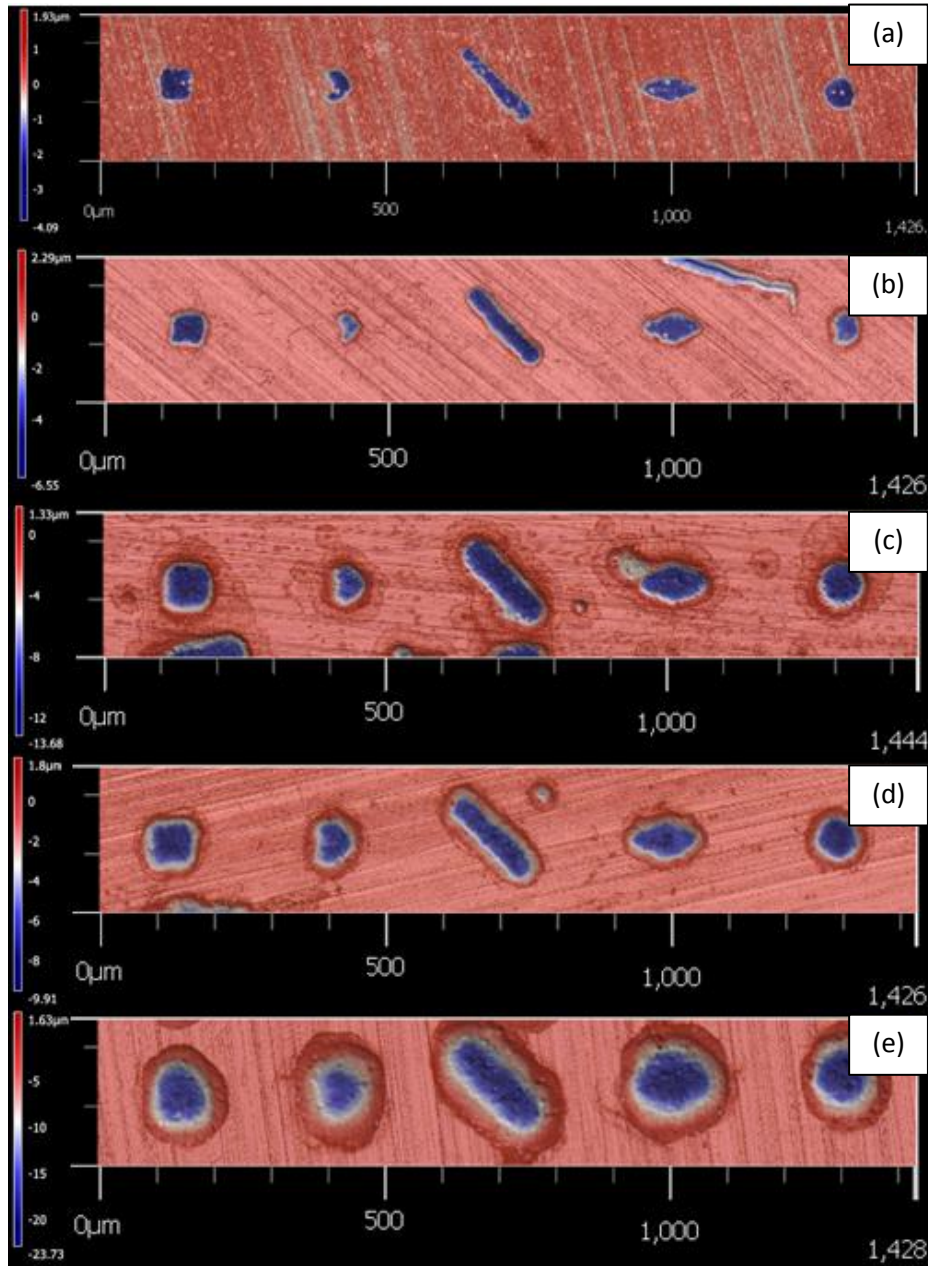


Figure 15: Demonstration of characteristic shape degradation and growth of the square, chevron, rectangle, diamond, and circle for the 5 (a), 8 (b), 13 (c), 19 (d), and 25 (e) minute etch times.

The only shapes that retained their semblance of their original shapes were the circular dimples, and the high-ratio rectangle, although only the high length to width ratio was still observable on the rectangle, all edges were etched and became rounded.

A common problem that was encountered with these experiments, however, was random undercut and randomly etched areas that were not selectively UV-exposed by the Nanoscribe. This problem can be observed on all experimental trials; an example can be seen in Figure 16.

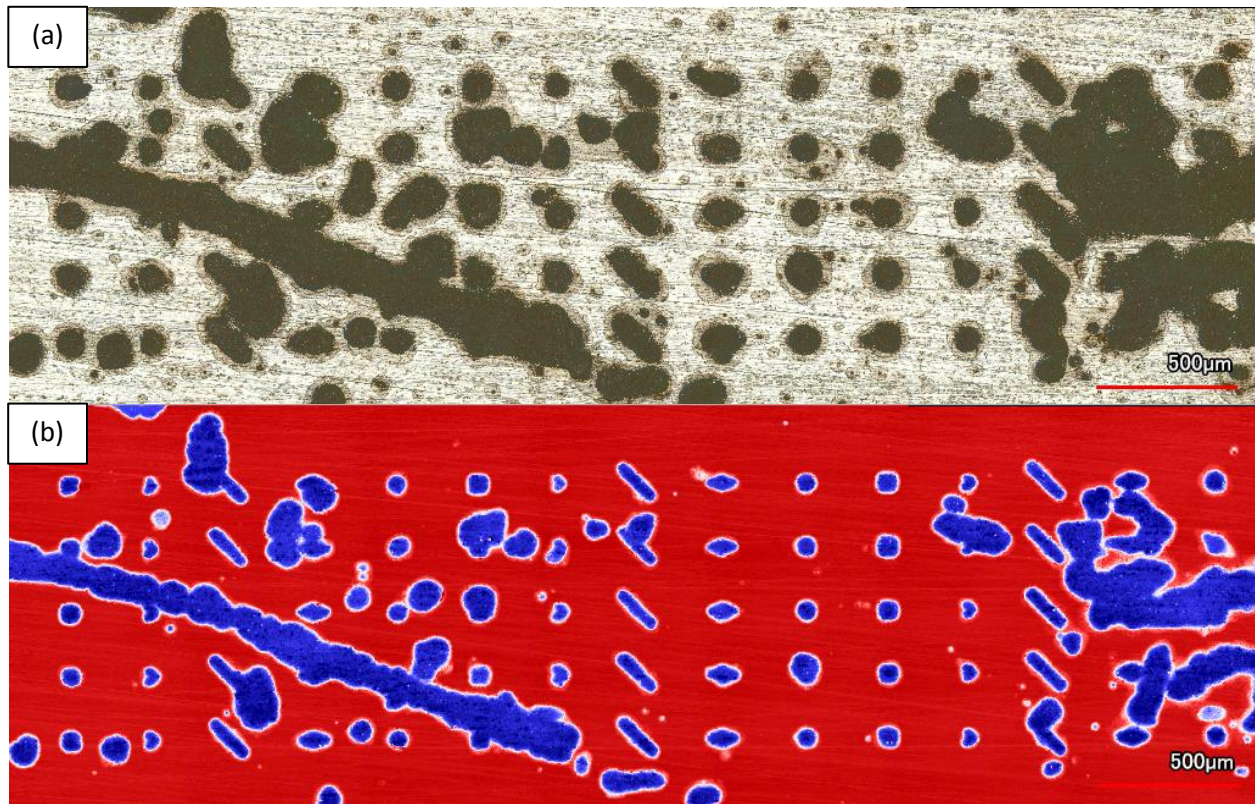


Figure16: An optical image (a) and a height map (b) of a piston ring section etched for 13 minutes demonstrating random etching and undercut problems.

## 4 CONCLUSIONS

The method of maskless photochemical etching developed in this experiment proves to be successful in etching specific shapes into the flat surface of nitrided stainless steel piston rings. Using the Nanoscribe to selectively expose the photoresist is a very accurate method that allows the freedom of designing the shape and size of the exposed area, for preliminary research. Dip coating the piston rings in AZ-9260 solutions was deemed as a universal method that can be applied to all surfaces of the piston ring, which will be used in future experiments.

The average etch depth of HCl on nitrided 17% Cr stainless steel piston rings was measured and shown to have a rate of about 0.7  $\mu\text{m}$  per minute. For 40x40  $\mu\text{m}$  squares, the side lengths increase at an average rate of 3.6  $\mu\text{m}$  per minute. For rectangles with initial dimensions of 15x150  $\mu\text{m}$ , the length increases at a rate of 3.7  $\mu\text{m}$  per minute, and the width increases at a rate of 4.36  $\mu\text{m}$  per minute. For diamonds with acute angles of 45 degrees and the initial distance between obtuse angles of 40  $\mu\text{m}$ , the distance between the obtuse angles increases at a rate of 3.8  $\mu\text{m}$  per minute.

When photochemically etching nitrided stainless steel piston rings, based on the measured etching rates, it is possible to control etch depth and size of the dimples. To do this, the final desired shape, size, and depth of the dimples must be selected, and based on various etching rates, the size and shape of the UV-exposed shape on the photoresist can be designed to create the desired outcome.

Any error or non-uniformity of these tests can be possibly attributed to the pre-existing texture on the surface of the piston ring, over-exposure of AZ-9260 based on age of the resist, or random error. The problem with unintended areas being etched needs for be investigated further.



## **5 FUTURE WORK**

### **5.1 Dimple Shape, Size, and Depth**

The results of this research provides a solid basis for future studies of further refining and applying the same techniques to selectively etch dimples of specific size, shape, and depth into piston rings. In order to do this and meet the future goals of the lab, these tests must be repeated at a much smaller scale, with the characteristic lengths of the shapes preferably being less than 10  $\mu\text{m}$ , possibly at the submicron scale.

More shapes should be tested and different printing parameters should be tested for each individual shape. Further analysis should be done on the etched shape to determine how the original shapes deform over time. If shape deformation can be accurately measured and characterized, this information can be applied to the initial UV-exposed shape in the photoresist, to compensate for the deformation and have etched dimples with the correct final shape.

### **5.2 Material and Application**

This technique of photochemical etching, like other techniques of surface engineering, can be universally applied to almost all substrates. These methods could be transferred not only to the curved surface of the piston ring with the right equipment, but also to other metals and surfaces that experience high friction and wear. We would like to test these techniques with aluminum and iron as well.

### **5.3 Friction Tests**

After dimple shape, size, and depth can be accurately controlled, friction tests should be performed to discover which variations of shape, size, and depth reduce the coefficient of friction the most.

## References

1. Writers S. One-third of car fuel consumption is due to friction loss. *UPI Space Daily*. 2012.
2. Holmberg K, Andersson P, Nylund N, Mäkelä K, Erdemir A. Global energy consumption due to friction in trucks and buses. *Tribol Int*. 2014;78:94-114.
3. Holmberg K, Andersson P, Erdemir A. Global energy consumption due to friction in passenger cars. *Tribol Int*. 2012;47:221-234.
4. Swigert AM, 1902, Chrysler Corporation. *The story of superfinish*. Detroit: Lynn Publishing Company; 1940.
5. Common practices in CYLINDER BORING, HONING, AND WALL FINISHING with suggestions and recommendations. [www.brushresearch.com/pdf/GB.pdf](http://www.brushresearch.com/pdf/GB.pdf). Updated 2006.
6. Nunney MJ. Engine lubrication, friction and wear. In: *Light and heavy vehicle technology*. Halley Court, Jordan Hill, Oxford OX2 8EJ: Heinemann Newnes; 1988:80-81.
7. Hsu S, Jing Y, Hua D, Zhang H. Friction reduction using discrete surface textures: Principle and design. *JOURNAL OF PHYSICS D-APPLIED PHYSICS*. 2014;47(33):335307.
8. Costil S, Lamraoui A, Langlade C, Heintz O, Oltra R. Surface modifications induced by pulsed-laser texturing—Influence of laser impact on the surface properties. *Appl Surf Sci*. 2014;288:542-549.
9. Gualtieri E, Borghi A, Calabri L, Pugno N, Valeri S. Increasing nanohardness and reducing friction of nitride steel by laser surface texturing. *Tribol Int*. 2009;42(5):699-705.
10. Vlădescu S, Ciniero A, Tufail K, Gangopadhyay A, Reddyhoff T. Looking into a laser textured piston ring-liner contact. *Tribol Int*. 2017;115:140-153.
11. Watanabe H, Tsuzaka H, Masuda M. Microdrilling for printed circuit boards (PCBs) - influence of radial run-out of microdrills on hole quality. *PRECISION ENGINEERING- JOURNAL OF THE INTERNATIONAL SOCIETIES FOR PRECISION ENGINEERING AND NANOTECHNOLOGY*. 2008;32(4):329-335.
12. Grabon W, Koszela W, Pawlus P, Ochwat S. Improving tribological behaviour of piston ring—cylinder liner frictional pair by liner surface texturing. *Tribol Int*. 2013;61:102-108.

13. Dunn A, Carstensen J, Wlodarczyk K, et al. Nanosecond laser texturing for high friction applications. *OPTICS AND LASERS IN ENGINEERING*. 2014;62:9-16.
14. Ali MY, Hung WNP. Comprehensive materials finishing. In: Vol 1. Elsevier; 2017:322-343.
15. Gietzelt T, Eichhorn L. *Mechanical micromachining by drilling, milling and slotting, micromachining techniques for fabrication of micro and nano structures.* ; 2012.
16. Marti J. Introduction to photolithography.  
[https://www.mnc.umn.edu/sites/g/files/pua586f/photolithography\\_graphical\\_material\\_v4.pdf](https://www.mnc.umn.edu/sites/g/files/pua586f/photolithography_graphical_material_v4.pdf)2018.
17. Wet chemical etching of metals and semiconductors. [https://cleanroom.byu.edu/wet\\_etch](https://cleanroom.byu.edu/wet_etch) 2018.
18. Walker P, Tarn WH. *CRC handbook of metal etchants*. Boca Raton: CRC Press; 1991.
19. Small KB, Englehart DA, Christman TA. A guide to etching specialty alloys for microstructural evaluation. <https://www.carttech.com/en/alloy-techzone/technical-information/manufacturing-guides/a-guide-to-etching-specialty-alloys-for-microstructural-evaluation>2018.
20. Weidmann E, Guesnier A, Taylor B. Metallographic preparation of stainless steel.  
<https://www.struers.com/-/media/Library/Brochures/English/Application-Note-Stainless-Steel.pdf?dmc=1&ts=20180213T1617431835>. Updated 20162018.
21. **Metallographic stainless steel etchants.** <https://www.metallographic.com/Metallographic-Etchants/Metallography-Stainless-steel-etchants.htm>2018.

## APPENDIX

### Equipment List

- 400 K (Developer for AZ-9260; prepared in a solution of 4:1, water to 400K)
- Dremel 8050-N/18 Micro 8V rotary tool with diamond tipped wheels for cutting the piston rings
- AZ-9260 (In a solution of 2:1, AZ-9260 to PGMEA)
- DI Water
- Dip coater
- Double sided tape
- Heat sinks (a copper bar was used to set the piston ring on while cutting)
- Microprime HP-Primer HMDS (ShinEtsumicroSi was the brand of HMDS primer used)
- Hexamethyldisilazane (HMDS)
- Hexane
- Hot plate
- Hydrochloric acid (34 - 37%, BDH ARISTAR® PLUS for trace metal analysis)
- Keyence Laser Scanner and MultiFileAnalyzer software
- Laboratory Grade Acetone
- Laboratory Grade Isopropyl Alcohol
- Multiple beakers (Each trial required 5 beakers)
- Nanoscribe and adjoining software
- Nitrided Piston Rings
- Piston Rings
- Propylene glycol methyl ether acetate (PGMEA)
- Proper safety equipment and chemical protective clothing
- Sonication bath